Climatic Change (2016) 137:217–230
DOI 10.1007/s10584-016-1663-8

Influence of the Indian Ocean Dipole on tree-ring $\delta^{18}O$ of monsoonal Southeast Tibet

Philipp Hochreuther[1] · Jakob Wernicke[1] · Jussi Grießinger[1] · Thomas Mölg[1] · Haifeng Zhu[2] · Lily Wang[3] · Achim Bräuning[1]

Received: 29 October 2015 / Accepted: 27 March 2016 / Published online: 7 April 2016

Abstract We present a newly developed, annually resolved tree-ring cellulose $\delta^{18}O$ chronology for the southeastern Tibetan Plateau (TP) from Sikkim larch (*Larix griffithii*), spanning between 1684 and 2012. Comparisons with local and regional climate data reveal strong positive correlations with monthly sunshine hours, temperature and daily temperature amplitude as well as strong negative correlations with relative humidity, vapor pressure, rain days per month and cloud cover of August. Relationships with local and regional tree-ring $\delta^{18}O$ chronologies are stable and highly significant. Over the 20th century, we find no long-term climatic trends. This is consistent with other tree-ring $\delta^{18}O$ chronologies of other tree species south of the Himalayas, but contrasts with results from isotope studies north of the Himalayas. This suggests stable macroclimatic flow patterns throughout the last centuries for the southern tree stands. In terms of large-scale climate dynamics, we find evidence of a significant 30-year wave influencing our tree-ring oxygen chronology, most probably induced by the Indian Ocean Dipole and influencing tree-ring oxygen isotope chronologies along the southeastern Himalaya and the southeastern rim of the TP. This pattern is spatially and temporarily consistent among the chronologies and has apparently strengthened during the last century. During periods of strong positive dipole mode activity, the dipole mode index shows positive correlations with the $\delta^{18}O$ of tree-rings on the southeastern TP.

✉ Philipp Hochreuther
philipp.hochreuther@fau.de

[1] Institute of Geography, University of Erlangen-Nuremberg, Wetterkreuz 15, 91058 Erlangen, Germany

[2] Key Laboratory of Tibetan Environment Changes and Land Surface Processes, Institute of Tibetan Plateau Research, Chinese Academy of Sciences, Beijing, China

[3] Institute of Geographical Sciences and Natural Resource Research, Chinese Academy of Sciences, Beijing, China

1 Introduction

The Asian Summer Monsoon (ASM) system, with the Indian- (ISM) and the East Asian summer monsoons (EASM) as its main branches, is the main moisture source for river discharge in South- and Southeast Asia (Ding and Wang 2005). As a consequence, knowledge about its strength and variability is of key importance for analyses and projections of water availability for the whole region (Immerzeel et al. 2010). With the Himalayas as a barrier and the Brahmaputra/Yarlung Tsangpo valley acting as an entry point for the moist air masses to proceed onto the Tibetan Plateau (TP), the extent and magnitude of the monsoonal footprint is highly variable from year to year (Böhner 2006; Tian et al. 2001a). Additionally, the westerlies have been recently identified as a major influence modulating the moisture input to the TP (Curio et al. 2015; Mölg et al. 2014). As the understanding of circulation variability has profited from more advanced models and improved scaling techniques (e.g. Mölg et al. 2014), long-term climate variability is still less clear. Stable oxygen isotope ratios (^{18}O /^{16}O) of lake sediments, ice cores, mollusk shells and tree-rings have been widely used as suitable proxies for the determination of moisture sources, −amounts and -pathways (Aggarwal et al. 2004; Mischke et al. 2010; Yao et al. 2012). However, proxy-based environmental reconstructions always incorporate the local conditions at the sampling site. Hence, it is sometimes challenging to relate variations of the proxy between different sampling sites and to distinguish common climatic forcing factors from local influences and peculiarities.

Driven by the thermal contrast between sea surfaces and the Asian continent, the coupled ocean-atmosphere systems of the tropics have a major influence on seasonal and annual characteristics of the ASM, including active and break phases. Especially the impact of the El Niño Southern Oscillation (ENSO) has been the focus of numerous studies (Collins 2005; Webster and Palmer 1997). Outside its main domain in the southern Pacific, ENSO also has profound influence on the Asian monsoon system (Kumar et al. 2006). For the southern Himalayan slopes and the southern TP, ENSO signals have been discovered in tree-ring series (Sano et al. 2011), but correlation strength varies in space and time (Liu et al. 2012). However, causal linkages between variations of ENSO, ISM and palaeoclimate proxies are not yet sufficiently understood. Another important climate mode influencing the ISM dynamics is the Indian Ocean Dipole (IOD, Saji et al. 1999). A positive IOD event starts with an upwelling of cold deep ocean water during the pre-monsoon season along the Indonesian coast. A gradient in sea surface temperature (SST) between the eastern (90° - 110°E; 0° - 10°S) and the western Indian Ocean (50° - 70°E; 10°N – 10°S) builds up, which is accompanied by southeastern trade wind anomalies. A warming of the western ocean region is amplifying the SST difference, which cumulates during the end of the monsoon season. While reduced convection over the eastern Indian ocean induces droughts at the Indonesian coasts, the shifted trade winds in combination with enhanced convection lead to a surplus of rainfall over the western Indian Ocean (Saji et al. 1999). Thus, being seasonally locked to the vegetation period, the IOD is a promising target to be studied with annually resolved tree-ring series. $\delta^{18}O$ from tree-ring cellulose has been recognized as a reliable proxy for hydroclimatic variability in the region (Grießinger et al. 2011; Sano et al. 2013; Wernicke et al. 2015). Despite of modifications through local moisture conditions, the $\delta^{18}O$ chronologies carry a regional signal, which is however not completely understood yet (Zhang et al. 2015). In this study, we therefore aim to explore potential influences of the IOD on the local and regional signals reflected in tree-ring $\delta^{18}O$ from the southeastern TP. We present the first *Larix griffithii* tree-

ring cellulose $\delta^{18}O$ chronology for the southeastern TP and explore its relationships to local and regional climate. We analyze the cyclicities and dominant frequencies of the chronology and discuss its relationship with other $\delta^{18}O$ series from the TP and with characteristics of the IOD climate mode.

2 Materials and methods

2.1 Study area and climate data

The study area is located on the southeastern TP, Xizang Autonomous Region, China (Fig. 1). The site is characterized by a dense forest of larch (*Larix griffithii*) and spruce (*Picea balfouriana*) growing below a terminal moraine dating from the Little Ice Age (LIA) at about 3700 m a.s.l. The upper timberline is located around 4500 m a.s.l. (Bräuning 2006).

The climate in the study region is strongly influenced by the ISM system during the vegetation period (May – September). Measurements from the nearby climate station at Bomi (distance approx. 10 km, 2750 m a.s.l., provided by the Chinese Meteorological Administration), were used for determining the relations of the chronology to climatic conditions. The instrumental measurement series is comparatively short (1960–2012), documenting a mean annual precipitation of 823 mm, with 75 % falling between April and September, and an annual mean temperature of 8.8 °C. To analyze spatio-temporal relationships, we additionally utilized gridded data (CRU TS 3.22) with a

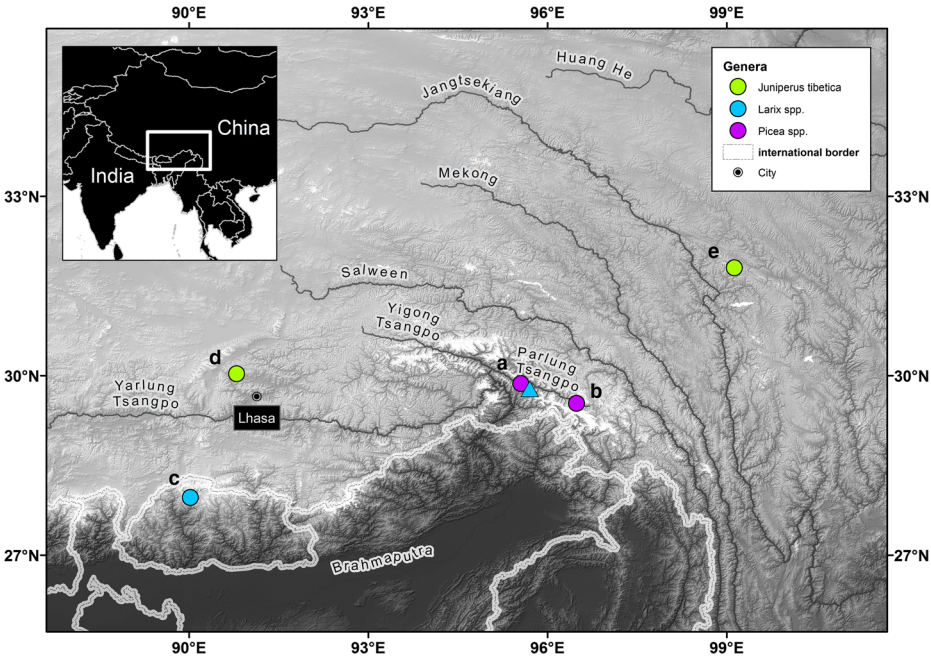

Fig. 1 Location of the study site Galongla (*blue triangle*) and other tree-ring inferred $\delta^{18}O$ chronologies (*circles*). **a** Bomi (Shi et al. 2012), **b** Ranwu Lake (Liu et al. 2013), **c** Bhutan (Sano et al. 2013), **d** Reting (Grießinger et al. 2011), **e** Lhamcoka (Wernicke et al. 2015)

0.5° resolution (1901–2012). The IOD index was derived from monthly SST differences (JAMSTEC: http://www.jamstec.go.jp/frcgc/research/d1/iod/iod/dipole_mode_index.html). To retrieve IOD event years (Fig. 6), we detrended the SST series of the western and eastern Indian Ocean from JAMSTEC separately through linear regression and standardized the dataset using its standard deviation (SD). Over multiple decades, such detrending is necessary since the IOD index calculation relies on anomalies from a long-term state mean (Saji et al. 1999). A deviation of 1 SD from the detrended mean was used as a threshold for determining IOD events.

2.2 Sampling and chronology development

First, 34 samples from 21 trees were taken during a field campaign in 1996, measured and averaged into a ring-width chronology (Bräuning 2006). This data set was expanded and updated with 22 cores from 18 trees of the same species (*Larix griffithii*) collected during a field campaign in 2012. The trees were cored at breast height using either a five or 12 mm diameter increment borer. Ring-width was measured employing a LINTAB 6 measuring system with TSAP-Win Software (Rinn 2003), which was also used for crossdating the ring-width series. Quality check of the measurements was performed with the statistical environment R (R Core team 2012), using functions from the dplR package (Bunn 2008) corresponding to COFECHA software (Holmes 1983). All ring-width series were averaged into the master chronology. For isotopic analysis, we selected five cores from different trees based on the following criteria: (1) length of the time series, (2) no occurrence of missing rings, and (3) high ring-width correlation and sign test (Gleichläufigkeit: GLK) values between each other and with the master chronology. To avoid any possible loss of information about the inter-tree variability and thus representativity (Dorado Liñán et al. 2011; McCarroll and Loader 2004), every ring of each core was cut and treated separately. The procedure recommended by Wieloch et al. (2011) was applied to extract alpha-cellulose from the whole wood, which was homogenized using an ultrasonic device (Laumer et al. 2009), freeze-dried and weighted into silver capsules. The $^{18}O/^{16}O$ ratio was determined using a Delta V Advantage Isotope Ratio Mass Spectrometer (Thermo Fischer Scientific Inc.) with a HEKAtech pyrolysis reactor. Single measurements were calibrated against IAEA 601/602 standards, with a maximum standard deviation of 0.2 ‰. The resulting individual isotope series were averaged into a chronology, whose strength and reliability was tested using RBar and Expressed Population Signal (EPS, Fig. 2). RBar is the mean inter-tree correlation coefficient, and is used in the calculation of the EPS to estimate how well a hypothetically perfect chronology with infinitite replication is represented in the developed chronology (Cook and Kairiūkštis 2010, 1989). The lengths of the individual isotope series are 272, 290, 311, 321 and 329 years, respectively (Fig. 2a).

2.3 Statistical treatment

Correlations between the $\delta^{18}O$ chronology and monthly climate data, including the current year and the year prior to growth as well as various seasonal means, were computed. From Bomi climate station, parameters included precipitation, minimum/mean/maximum temperatures, relative humidity, sunshine hours, vapor pressure and wind speed, spanning the period 1960–2012. Correlations with CRU.TS data v. 3.22 included precipitation, minimum/mean/

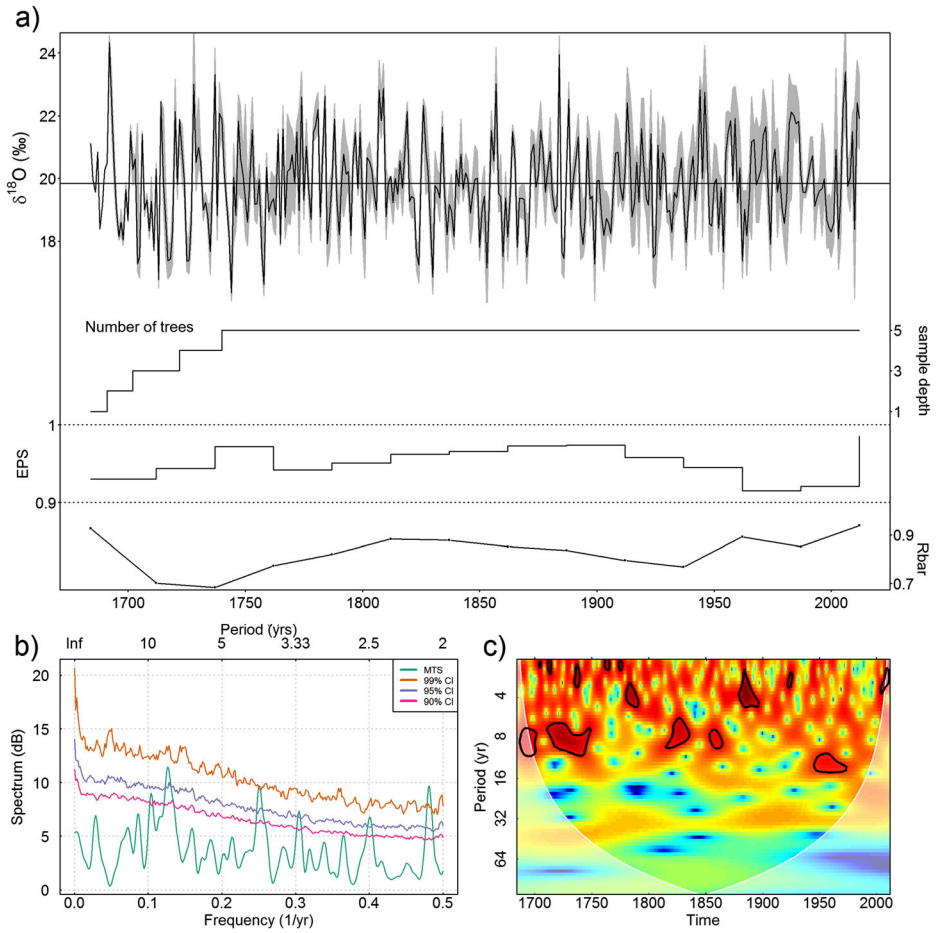

Fig. 2 Time series analysis: **a** the 328-year larch tree-ring $\delta^{18}O$ series with sample sizes, running EPS and Rbar values computed over 50 years lagged by 25 years; *grey shadow* represents the difference between minimum and maximum $\delta^{18}O$ content of the individual series, *horizontal black line* indicates the chronology mean (19.8 ‰). **b** Multi-taper spectrum (MTS, Mann and Lees 1996) of the record, with 90, 95 and 99 % confidence levels (CI: confidence intervals) inferred from red noise spectra; **c** wavelet transform of the $\delta^{18}O$ chronology, with significant ($p < 0.01$) periods highlighted by solid *black lines*

maximum temperatures, potential evapotranspiration, rain days per month, vapor pressure, cloud cover, and diurnal temperature range. Statistical and frequency analyses were carried out using R; the dplR package was used for crossdating the isotope series and chronology building, as well as the computation and visualization of the red noise spectra and wavelets; multi-taper spectra were computed using the package multitaper (Rahim 2014). Significance levels for the moving correlation were computed using Monte Carlo-simulations with 1000 runs against normally distributed random numbers. To reveal possibly hidden connections in time-frequency space, we applied wavelet coherence analysis using the R package WaveletComp (Roesch and Schmidbauer 2014). The coherence method compares the wavelet transforms of two time series (Grinsted et al. 2004).

3 Results and discussion

3.1 Chronology statistics

The Galongla $\delta^{18}O$ chronology is defined by a global minimum/maximum of 16.4/24.3 ‰ (1744/1692), resulting in a total amplitude of 7.9 ‰. The mean is 19.8 ‰ with an annual standard deviation of ±1.42 ‰. The trees within the chronology show high synchronicity, as expressed by a mean GLK of 0.81 and a global EPS of 0.95, indicating a strong common forcing and a reliable mean $\delta^{18}O$ chronology. The chronology mean is considerably lower than that of nearby spruce chronologies (Shi et al. 2012 and Liu et al. 2013), differing by 3.23 ‰ and 5.03 ‰, while differences of standard deviations are negligible (0.009 ‰ and 0.1 ‰). The large difference between the means of the two spruce chronologies might arise from the difference in altitude of the sites (2760 m and 4200 m a.s.l.) and physiological differences between the species, as well as microclimatic inhomogenities. Variations in the average $\delta^{18}O$ values between *Larix* and *Picea* are consistent with studies from the southern Himalayas: for instance, Sano et al. (2013) found 3.32 ‰ difference between nearby sites in Bhutan, while Li et al. (2011) reported 1.5 ‰ in northern China.

The MTS reveals significant wavelengths of 8, 4, 3.3, 2.5 and 2.2 years, while only the latter passes the 99 % confidence level inferred from the red noise spectra (Fig. 2b). Fluctuations in the domain of two to three years could originate from the Tropospheric Biennial Oscillation (Meehl and Arblaster 2001), but may also be assumed being white noise for annually resolved time series. The 4- and 8-year frequencies can be found mainly prior to 1880 (Fig. 2c).

3.2 Oxygen isotope - climate relationships

August sunshine hours exhibit the highest correlation ($r = 0.68$, $p < 0.001$, Fig. 3) with the $\delta^{18}O$ data, and illustrate the dependence of tree respiration on warm and sunny conditions. As August is clearly the key month for determining the isotopic ratio of oxygen in the cellulose of the trees, highly significant correlations also occur (in descending order) with relative humidity, maximum temperature, and vapor pressure. Lower, but still significant, influence can be attributed to precipitation. The strongest negative correlations with precipitation amount are achieved for July and August ($r = -0.38$, $p < 0.05$), which is in good accordance with other regional isotope series (Grießinger et al. 2011; Wernicke et al. 2015).

The relationship between the $\delta^{18}O$ chronology and the climatic variables is physically consistent: maximum temperature in August is highly dependent on direct insolation and thus monthly sunshine hours. Warm and sunny conditions enhance evapotranspiration which leads, according to the Craig-Gordon model, to a depletion of ^{18}O due to leaf water fractionation (Roden 2005). According to Kahmen et al. (2011), the process is not soley controlled by temperature (insolation) or humidity, but rather by an equal influence of both climate elements. Hence, the leaf-to air vapor pressure difference (VPD) integrates temperature and rH in one variable that reliably determines the $\delta^{18}O$ in plants cellulose.

3.3 Regional scope of the climatic signal

To assess macroclimatic imprints on the $\delta^{18}O$ of the trees, we correlated our data with the 0.5° gridded CRU 3.22 dataset (1901–2012), see Fig. 4. Field correlations exhibit a regional-scale signal that is reflected by the Galongla tree-ring $\delta^{18}O$ chronology. High-frequency variations

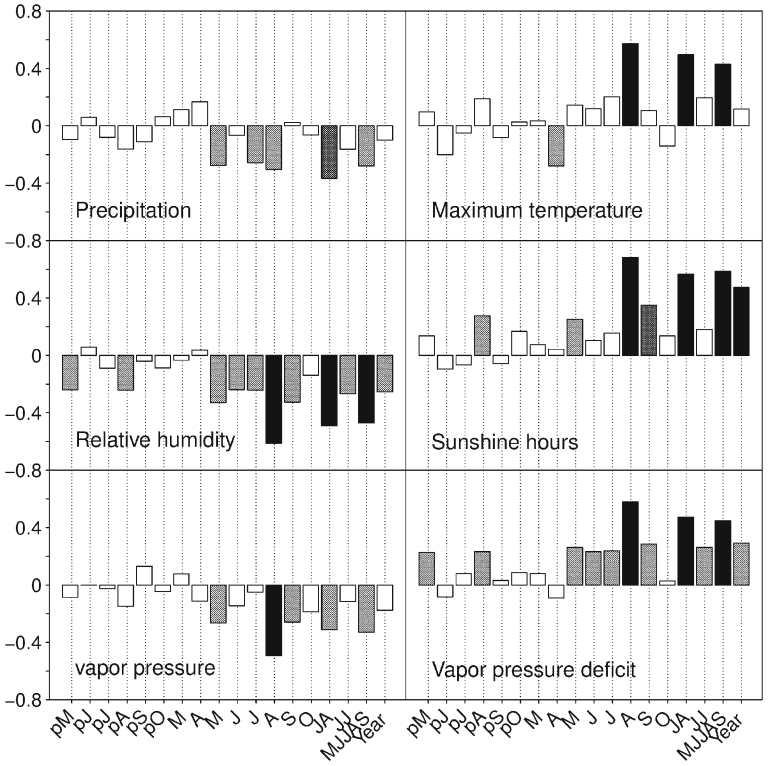

Fig. 3 Correlations between the annual Galongla tree-ring $\delta^{18}O$ values and monthly to seasonal values of precipitation, maximum temperature, relative humidity, sunshine hours, vapor pressure and –deficit data between 1960 and 2012. Months of the previous growth year start with p. *Grey/black bars* indicate significant/highly significant values ($p < 0.05/0.01$)

in the time series are consistent with those of maximum temperature (Fig. 4a) and daily temperature variations (4b) of August throughout large parts of the southern-, southeastern, and eastern TP, while negative correlations with precipitation amount (4c) and cloud cover (4d) exhibit similar spatial patterns. Although especially the latter variables are related to monsoon strength during August, the correlation pattern shows a west-east-orientation, stretching until the East China Sea and Japan. A clear opposite correlation pattern is apparent between the southern−/southeastern TP and northeast China/eastern Russia, central Asia and west/northwest India. Similar patterns were also found by Wernicke et al. (2015) for ERA Interim derived summer relative humidity data (July–August) in 500 hPa and 300 hPa levels. In particular for northwest India, the opposite correlation could indicate a potential mid-latitude influence on the monsoon climate. Cold anomalies over northwestern India and Pakistan typically weaken the ISM intensity (Saeed et al. 2011), and thus might promote dry (and sunshine-rich) conditions on the TP, including our study area. This needs to be elaborated in more detail in the future, but seems a reasonable preliminary explanation.

We additionally tested the spatial correlations for the whole monsoon season (May–September, data not shown). The results show the same patterns as for August, whereas the correlations are 0.1 lower on average, but still highly significant. The lower average probably results from the non-significant influence of the early monsoon months affecting the correlation results.

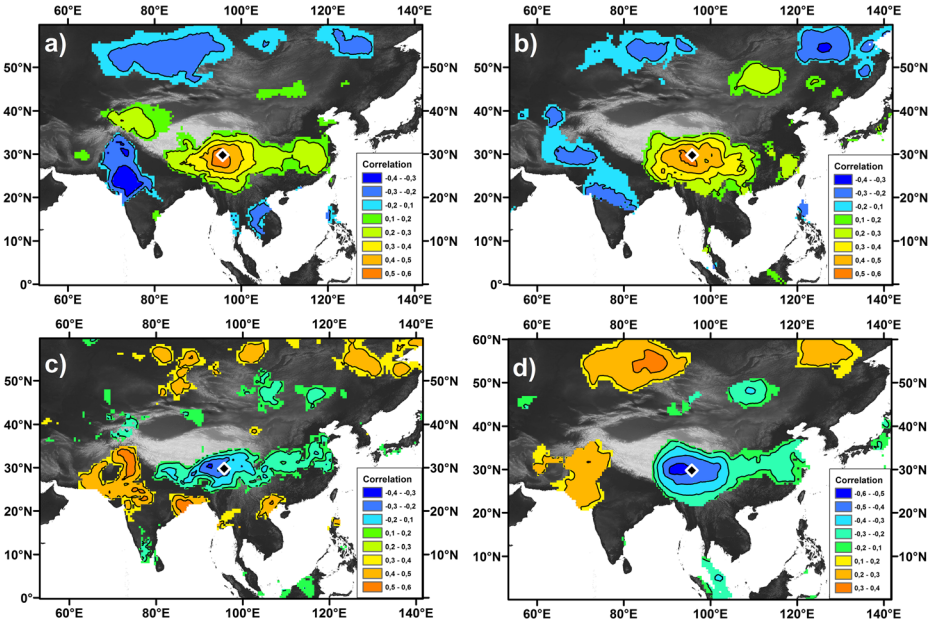

Fig. 4 Field correlations ($p < 0.1$) of Galongla tree-ring cellulose $\delta^{18}O$ (*black diamond*) with **a** maximum temperature, **b** daily temperature range, **c** precipitation and **d** cloud cover of CRU.TS 3.22 data for August between 1901 and 2012. Correlations weaker than ±0.1 are not displayed; $p < 0.01$ with 11 degrees of freedom: 0.24

3.4 Relationships with the Indian Ocean Dipole (IOD)

Our study site Galongla is located within the main ISM-related moisture pathway entering the TP through the Brahmaputra valley (Curio et al. 2015; Tian et al. 2001b). Therefore, the moisture availability for the trees should be strongly controlled by ISM variations. Although a precondition for its formation is the temperature difference between the Asian land mass and the surrounding oceans (Kumar et al. 1999), the strength and duration is highly variable on timescales varying between months and centuries.

The ENSO has a strong influence on the monsoon system (Kumar et al. 2006; Wu et al. 2012), but its effect has been found to decay during the last decades (Kumar et al. 1999). Unlike ENSO, which is seasonally independent, such that events may occur during boreal winter or summer (or even last for several years), the IOD is seasonally phase-locked and has been discovered as a major factor influencing the strength and seasonal characteristics of the Asian monsoon system (Yang et al. 2010). While positive events enhance late summer−/autumn rainfall in southeast China through intensified easterly- (JJA)/westerly (SON) lower tropospheric winds, the effect is contrary for the southern- and southeastern TP (Qiu et al. 2014).

To test the possible connection between the IOD during the monsoon season (MJJAS) and the Galongla tree-ring $\delta^{18}O$ chronology, we used simple and moving correlation with different windows of five, ten and 30 years. Even if the mean correlation is weak and insignificant ($r = 0.19$, $p > 0.1$), the 10-year moving correlation fluctuates with a cyclicity of 30 years over the whole study period (Fig. 5a). Due to the shortness of the correlation window, correlation values reach significant levels only around 1985. In addition to an increase in correlation

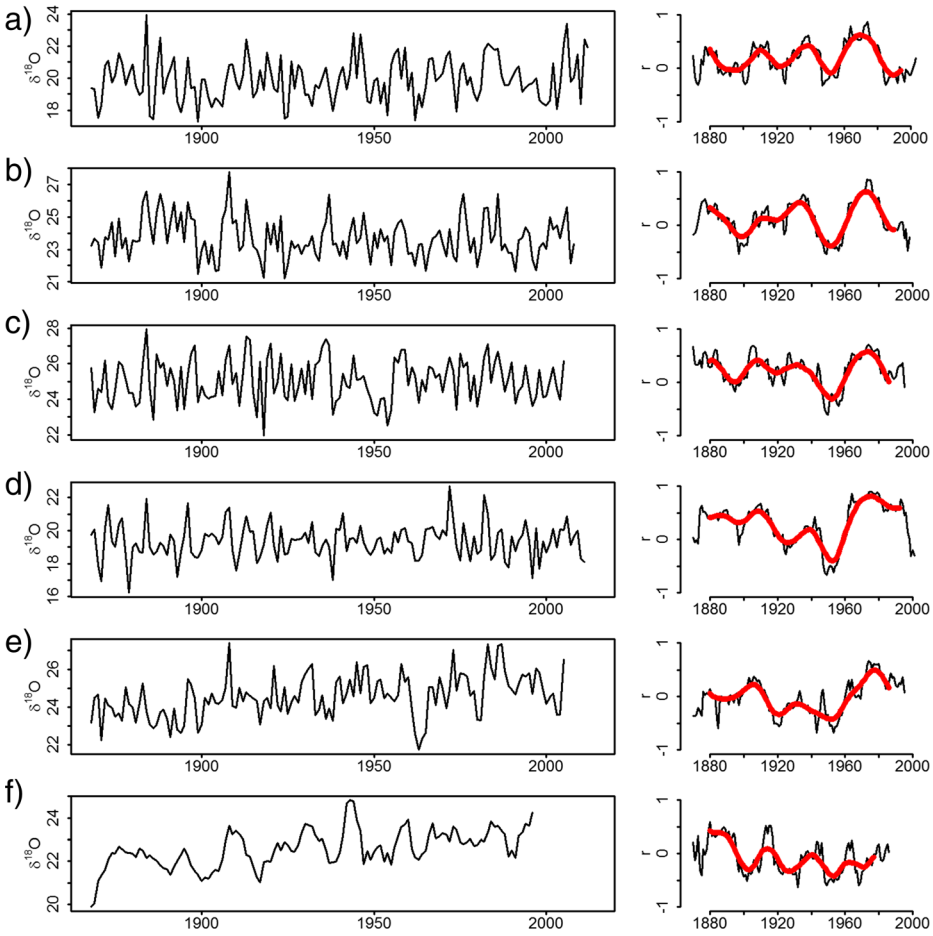

Fig. 5 Comparison of the tree-ring $\delta^{18}O$ series of **a** this study, **b** Ranwu Lake (Liu et al. 2013), **c** Bomi (Shi et al. 2012), **d** Bhutan (Sano et al. 2013), **e** Reting (Grießinger et al. 2011) and **f** Lhamcoka (Wernicke et al. 2015). Left column shows raw $\delta^{18}O$ chronologies between 1870 and 2014 (when Hadley SSTs as used by JAMSTECH are available). Right column shows moving correlations between the $\delta^{18}O$ chronologies and Hadley SST-derived IOD index for the monsoon season (May – September) using a 10-year window, smoothed by a robust locally weighted regression filter (LOWESS) with 0.2 rigidity

strength, the frequency is lowering, from exactly 30 years at the beginning of the 20th century to ~40 years in more recent years. This is in line with the analysis of Mölg et al. (2006), who found the same wavelength in the second principal component (PC) of the Indian Ocean SST's Empirical Orthogonal Functions (EOF). This PC, which reflects the IOD zonal mode, also oscillates with a decreasing frequency towards the end of the 20th century.

We performed the moving correlation analysis also for the neighboring spruce chronologies (Liu et al. 2013, Shi et al. 2012), the Bhutan larch chronology of Sano et al. (2013), and the more arid juniper chronologies of Grießinger et al. (2011) and Wernicke et al. (2015). As shown in Fig. 5, the 30-year wave is present in all moving correlation time series of the southeastern TP (a-c), as well as in the Bhutan series (d). This strongly supports our assumption of the IOD as an important influence on climate variability in the region, most likely through moisture variability. However, the correlation pattern for Reting (e) is less

evident, though still recognizable. Lhamcoka (f) exhibits a slightly shorter frequency with coefficients around zero, the influence of the IOD might therefore be constrained by increasing continentality, or the increasing influence of the EASM. These findings underline the role of the Himalayas as a moisture barrier (Maussion et al. 2014).

To investigate possible reasons for the fluctuating decadal correlation, we compared the fluctuations in time-frequency space of the IOD to those of the isotope series using wavelet coherence (Fig. 6c). Since the running correlation in terms of amplitude and period length match between the sites in SE Tibet, we averaged the three isotope series of Bomi, Ranwu Lake and Galongla into one mean SE Tibet $\delta^{18}O$ chronology. The 30-year wave does not appear in neither the wavelet transform of the Dipole Mode Index (DMI) and SE Tibet $\delta^{18}O$ chronology (plots not shown), nor are the wavelets of the DMI and the $\delta^{18}O$ chronology

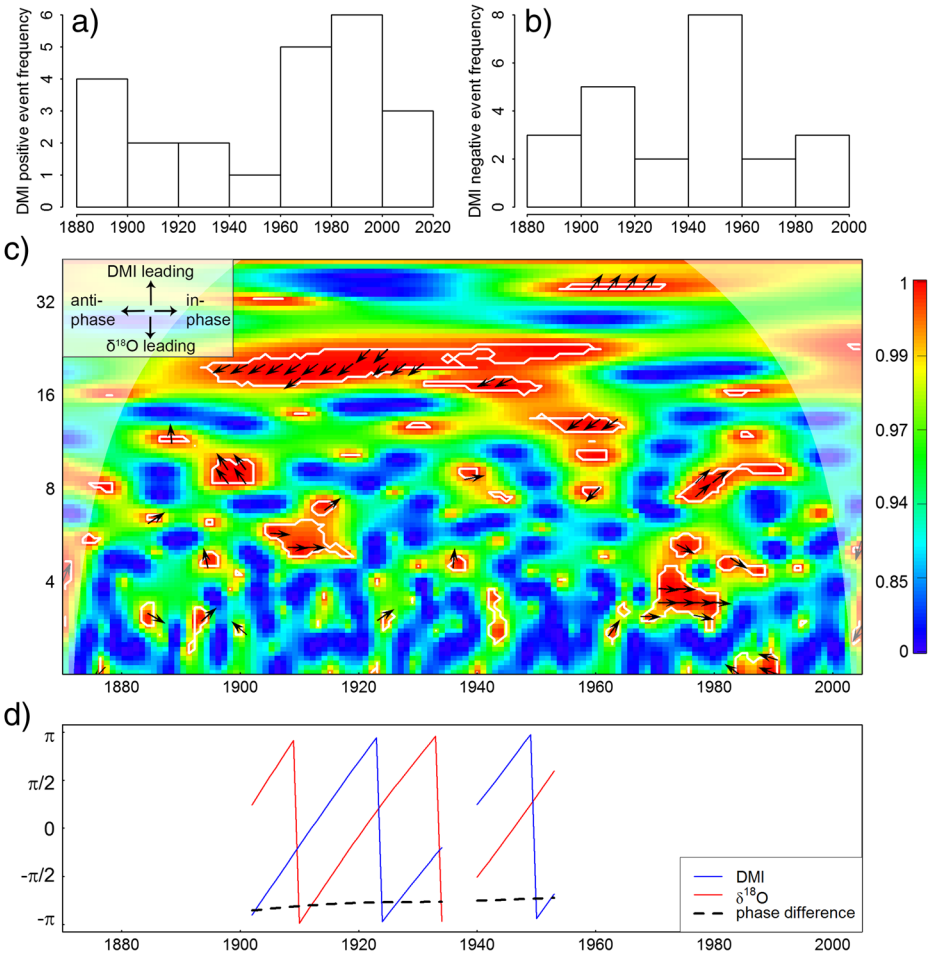

Fig. 6 **a** Frequency of positive IOD events for 20-year intervals; **b** Frequency of negative IOD events for 20-year intervals; **c** Wavelet coherence using the wavelet transforms of the mean SE Tibet $\delta^{18}O$ chronology and the DMI. Phase arrows pointing right indicate in-phase behavior, arrows pointing up/down indicate a phase lead of the DMI/$\delta^{18}O$ phase. Left-pointing arrows indicate an anti-phase. d) Comparison plot of phases for the 20-year component of the two time series. Between 1900 and 1960, both time series show a phase delay of almost π, indicating anti-phasic characteristics

coherent at this frequency. Contrasting, both time series seem to be in antiphase at a frequency band between 20 and 25 years (significant ($p < 0.01$) coherence highlighted by gray solid lines in Fig. 6c), as indicated by the arrows showing a phase delay of almost π (Fig. 6d). Covering almost the entire common period (1870–2010), this explains the average low correlation between the DMI and the $\delta^{18}O$ series. The significant band weakens only for periods between 1880 and 1900 and after 1960. During the latter period, a significant in-phase frequency of four years replaces the pattern, explaining the high running correlations between 1970 and 1990. Since 1960, the frequency of positive IOD events has increased (Abram et al. 2007, Fig. 6a). The detrended DMI also shows an enhanced frequency of positive IOD events before 1900 (Fig. 6a), yet not reaching the level of the recent decades. It is therefore probable that a high frequency of positive IOD events leads to high correlations between the DMI and tree-ring $\delta^{18}O$. The frequency of negative events, on the other hand, does not seem to be of importance to this relationship. This implies that the IOD does have a significant influence on the tree-ring $\delta^{18}O$ of SE Tibet and the Himalayas, but the influence is likely only imprinted in the tree-rings during the event year and maybe the year after through storage effects and remobilization of carbohydrates. Therefore, the correlation is only strong when a certain frequency (approximately 3–4 per decade) of positive IOD events is reached. Otherwise, the tree-ring $\delta^{18}O$ is likely more influenced by other climatic modes, or regional climatic factors.

Ashok et al. (2001) investigated the relationship between All-ISM rainfall amount (ISMR, Parthasarathy et al. 1995), the IOD and ENSO 3 region SSTs for the period 1958–1997 using an atmospheric general circulation model (AGCM). They found a reversal of the correlation between the ISMR and both variables between 1965 and 1980, implying that during times of low IOD anomalies, ENSO dominates the influences on monsoonal precipitation amounts. Our correlation analysis for ENSO 3 SST - tree-ring $\delta^{18}O$ does not reflect such a relationship. This difference might result from the fact that the $\delta^{18}O$ tree-ring chronology as a climate proxy is mirroring several climatic, physiological and site-specific influences. Additionally, the precipitation amount at Bomi climate station does not reflect the ISMR ($r = -0.13$, $p > 0.1$), but is expected to represent the northeast Indian monsoon, locally modified by the extreme topography (Curio et al. 2015). The strongest positive correlations of our chronology are found with insolation-driven parameters (amount of sunshine hours, maximum temperature, and diurnal temperature range). During positive IOD events, in early summer (May/June), SSTs in the eastern Indian Ocean are lowered due to upwelling of cold saline deep ocean water. Cold ocean water diminishes sea water evaporation, resulting in reduced convective activity. Hence, the cloud cover can be expected to decrease, leading to increased hours of sunshine and lower relative humidity. As a consequence, leaf water fractionation is enhanced, leading to $\delta^{18}O$ enrichment through stomatal closure.

The complex interaction between ISM(R), ENSO and IOD is still difficult to disentangle and a matter of ongoing research. The ENSO and IOD are embedded in the Walker circulation: often, a positive IOD phase in boreal autumn precedes a La Niña event, whereas negative phases precede El Niños (Izumo et al. 2010). Accordingly, Park et al. (2010) discovered that the ENSO influence on the ISM results in weaker monsoonal precipitation in the year before an ENSO event. They also reported increased precipitation amounts during the following late-monsoon season. While the precipitation amount itself may not influence the tree-ring cellulose $\delta^{18}O$ directly (Gray and Thompson 1976; Epstein et al. 1977), an effect can be expected a) via the rainout of the heavier isotope during increased precipitation events, the so-called amount effect (Hoffmann and Heimann 1997), b) change of the isotopic composition of convective air parcels over the Bay of Bengal due to upwelling of cold deep-sea water during

positive IOD events (Bigg and Rohling 2000), and c) increased relative humidity due to high amounts of precipitation, resulting in a low vapor pressure deficit and thus hampered discrimination against the lighter isotopes (Dansgaard 1964). An additional influence might arise from the dependency of the $\delta^{18}O$ leaf water fractionation from the isotopic composition of the water vapor itself (Gessler et al. 2013). Advection of moist air parcels with different source water signals might vary the source water $\delta^{18}O$ content. However, as the flow direction during the monsoon season on the southern Himalayan slope as well as on the southeastern TP can be assumed relatively stable (Hren et al. 2009), this effect may play a minor role.

4 Conclusions

Our *Larix* $\delta^{18}O$ chronology reflects the influence of multiple climate variables during the peak of the summer monsoon season on the southeastern TP. The absence of a long-term trend in our chronology suggests stable monsoon conditions in SE Tibet since the late 17th century, which is in accordance with findings from local tree-ring $\delta^{18}O$ chronologies. The highest correlations with sunshine hours and relative humidity in August indicate a strong influence during the monsoon season. Spatiotemporal analyses indicate a significant influence of regional-scale maximum temperature and daily temperature variations (which possibly reflect relative humidity) on the southern and southeastern TP and central China during August on $\delta^{18}O$ in the tree-rings. Additionally, negative correlations of $\delta^{18}O$ with August precipitation and cloud cover also show a west-east pattern, which links our study site to climate variations from the southern Himalayan rim to central and east China.

Fluctuating correlations with the Indian Ocean zonal mode reveal a significant 30- to 40-year frequency. These findings are in accordance with climate modelling results and thus show that proxies are suitable to better evaluate modelling approaches, and to constrain climate projections. Results from wavelet coherence analysis suggest that tree-ring $\delta^{18}O$ is highly correlated with the IOD index during decades with a high frequency of positive IOD events. Proxy studies aiming at the detection of major climate modes in the Indiopacific region should, therefore, consider the changing influence of the IOD during the times measured climate data are available. Since the IOD index is based on the SST differences in the tropical Indian Ocean, and the ISM is the main moisture source for the southern Himalayas and the southeastern TP during the monsoon season, we present further evidence of the IOD influence on the variability of monsoon moisture on the southeastern TP.

Acknowledgments The authors are indebted to the German Research Foundation (DFG BR 1895/21-1) for funding. We thank Dr. Fan Zexin for contributing climate data, and Dr. Masaki Sano and Dr. Qi-Bin Zhang for providing their $\delta^{18}O$ series.

References

Abram NJ, Gagan MK, Liu Z, Hantoro WS, McCulloch MT, Suwargadi BW (2007) Seasonal characteristics of the Indian Ocean Dipole during the Holocene epoch. Nature 445(7125):299–302

Aggarwal PK, Fröhlich K, Kulkarni KM, Gourcy LL (2004) Stable isotope evidence for moisture sources in the asian summer monsoon under present and past climate regimes. Geophys Res Lett 31(8):L08203

Ashok K, Guan Z, Yamagata T (2001) Impact of the Indian Ocean Dipole on the relationship between the Indian monsoon rainfall and ENSO. Geophys Res Lett 28(23):4499–4502

Bigg GR, Rohling EJ (2000) An oxygen isotope data set for marine waters. J Geophys Res 105(C4):8527
Böhner J (2006) General climatic controls and topoclimatic variations in central and high Asia. Boreas 35(2): 279–295
Bräuning A (2006) Tree-ring evidence of 'Little ice Age' glacier advances in Southern Tibet. The Holocene 16(3): 369–380
Bunn AG (2008) A dendrochronology program library in R (dplR). Dendrochronologia 26(2):115–124
Collins M (2005) El Niño- or La Niña-like climate change? Clim Dyn 24(1):89–104
Cook E, Kairiūkštis L (2010, 1989) Methods of dendrochronology: Applications in the environmental sciences. Kluwer Academic Publishers, Dordrecht, Netherlands
Curio J, Maussion F, Scherer D (2015) A 12-year high-resolution climatology of atmospheric water transport over the Tibetan Plateau. Earth Syst Dyn 6(1):109–124
Dansgaard W (1964) Stable isotopes in precipitation. Tellus 16(4):436–468
Ding Q, Wang B (2005) Circumglobal Teleconnection in the Northern Hemisphere summer. J Clim 18(17): 3483–3505
Dorado Liñán I, Gutiérrez E, Helle G, Heinrich I, Andreu-Hayles L, Planells O, Leuenberger M, Bürger C, Schleser GH (2011) Pooled versus separate measurements of tree-ring stable isotopes. Sci Total Environ 409(11):2244–2251
Epstein S, Thompson P, Yapp CJ (1977) Oxygen and hydrogen isotopic ratios in plant cellulose. Science 198(4323):1209–1215
Gessler A, Brandes E, Keitel C, Boda S, Kayler ZE, Granier A, Barbour M, Farquhar GD, Treydte K (2013) The oxygen isotope enrichment of leaf-exported assimilates–does it always reflect lamina leaf water enrichment? New Phytol 200(1):144–157
Gray J, Thompson P (1976) Climatic information from 18O/16O ratios of cellulose in tree rings. Nature 262(5568):481–482
Grießinger J, Bräuning A, Helle G, Thomas A, Schleser G (2011) Late Holocene Asian summer monsoon variability reflected by δ18 O in tree-rings from Tibetan junipers. Geophys Res Lett 38(3):L03701
Grinsted A, Moore JC, Jevrejeva S (2004) Application of the cross wavelet transform and wavelet coherence to geophysical time series. Nonlinear Process Geophys 11(5/6):561–566
Hoffmann G, Heimann M (1997) Water isotope modeling in the Asian monsoon region. Quat Int 37:115–128
Holmes RL (1983) Computer -assisted quality control in tree -ring dating and measurement. Tree-Ring Bull 43: 69–78
Hren MT, Bookhagen B, Blisniuk PM, Booth AL, Chamberlain CP (2009) δ18O and δD of streamwaters across the Himalaya and Tibetan Plateau: Implications for moisture sources and paleoelevation reconstructions. Earth Planet Sci Lett 288(1–2):20–32
Immerzeel WW, van Beek LP, Bierkens MF (2010) Climate change will affect the asian water towers. Science 328(5984):1382–1385
Izumo T, Vialard J, Lengaigne M, de Boyer Montegut C, Behera SK, Luo J, Cravatte S, Masson S, Yamagata T (2010) Influence of the state of the Indian Ocean Dipole on the following year's El Niño. Nat Geosci 3(3): 168–172
Kahmen A, Sachse D, Arndt SK, Tu KP, Farrington H, Vitousek PM, Dawsona TE (2011) Cellulose $\delta^{18}O$ is an index of leaf-to-air vapor pressure difference (VPD) in tropical plants. PNAS 108(5):1981–1986
Kumar KK, Rajagopalan B, Cane M (1999) On the Weakening relationship between the Indian monsoon and ENSO. Science 284(5423):2156–2159
Kumar KK, Rajagopalan B, Hoerling M, Bates G, Cane M (2006) Unraveling the mystery of Indian monsoon failure during El Niño. Science 314(5796):115–119
Laumer W, Andreu L, Helle G, Schleser G, Wieloch T, Wissel H (2009) A novel approach for the homogenization of cellulose to use micro-amounts for stable isotope analyses. Rapid Commun Mass Spectrom 23(13): 1934–1940
Li Q, Nakatsuka T, Kawamura K, Liu Y, Song H (2011) Regional hydroclimate and precipitation δ18O revealed in tree-ring cellulose δ18O from different tree species in semi-arid Northern China. Chem Geol 282(1–2): 19–28
Liu X, An W, Treydte K, Shao X, Leavitt S, Hou S, Chen T, Sun W, Qin D (2012) Tree-ring δ18O in Southwestern China linked to variations in regional cloud cover and tropical sea surface temperature. Chem Geol 291:104–115
Liu X, Zeng X, Leavitt SW, Wang W, An W, Xu G, Sun W, Wang Y, Qin D, Ren J (2013) A 400-year tree-ring δ18O chronology for the southeastern Tibetan Plateau: Implications for inferring variations of the regional hydroclimate. Glob Planet Chang 104:23–33
Mann ME, Lees JM (1996) Robust estimation of background noise and signal detection in climatic time series. Clim Chang 33(3):409–445

Maussion F, Scherer D, Mölg T, Collier E, Curio J, Finkelnburg R (2014) Precipitation seasonality and variability over the Tibetan Plateau as resolved by the high Asia reanalysis. J Clim 27(5):1910–1927
McCarroll D, Loader NJ (2004) Stable isotopes in tree rings. Quat Sci Rev 23(7–8):771–801
Meehl GA, Arblaster JM (2001) The tropospheric Biennial Oscillation and Indian monsoon rainfall. Geophys Res Lett 28(9):1731–1734
Mischke S, Aichner B, Diekmann B, Herzschuh U, Plessen B, Wünnemann B, Zhang C (2010) Ostracods and stable isotopes of a late glacial and Holocene lake record from the NE Tibetan Plateau. Chem Geol 276(1–2): 95–103
Mölg T, Renold M, Vuille M, Cullen NJ, Stocker TF, Kaser G (2006) Indian Ocean zonal mode activity in a multicentury integration of a coupled AOGCM consistent with climate proxy data. Geophys Res Lett 33(18):L18710
Mölg T, Maussion F, Scherer D (2014) Mid-latitude westerlies as a driver of glacier variability in monsoonal high Asia. Nat Clim Chang 4(1):68–73
Park H, Chiang JCH, Lintner BR, Zhang GJ (2010) The Delayed effect of major El Niño events on Indian monsoon rainfall. J Clim 23(4):932–946
Parthasarathy B., Munot A.A., Kothawale D.R. (1995) Monthly and seasonal rainfall series for all-India homogeneous regions and meteorological subdivisions: 1871–1994. Research Report, RR-065. Indian Institute of Tropical Meteorology, Pune
Qiu Y, Cai W, Guo X, Ng B (2014) The asymmetric influence of the positive and negative IOD events on China's rainfall. Sci Rep 4:4943
R Core team (2012) R: A language and environment for statistical computing. R Foundation for Statistical Computing, Wien
Rahim K (2014) Applications of multitaper Spectral analysis to Nonstationary data. Queen's University, Thesis
Rinn F (2003) TSAP-Win Professional: time series analysis and Presentation for dendrochronology and related Applications. RINNTECH, Heidelberg
Roden JS (2005) Carbon and oxygen isotope ratios of tree ring cellulose along a precipitation transect in Oregon, United States. J Geophys Res 110(G2)
Roesch A, Schmidbauer H (2014) WaveletComp: computational wavelet analysis: R package version 1.0 http://CRAN.R-project.org/package=WaveletComp. Accessed 17 Feb 2016
Saeed S, Müller WA, Hagemann S, Jacob D (2011) Circumglobal wave train and the summer monsoon over Northwestern India and Pakistan: the explicit role of the surface heat low. Clim Dyn 37(5–6):1045–1060
Saji NH, Goswami BN, Vinayachandran PN, Yamagata T (1999) A dipole mode in the tropical Indian Ocean. Nature 401(6751):360–363
Sano M, Ramesh R, Sheshshayee M, Sukumar R (2011) Increasing aridity over the past 223 years in the Nepal Himalaya inferred from a tree-ring δ18O chronology. The Holocene 22(7):809–817
Sano M, Tshering P, Komori J, Fujita K, Xu C, Nakatsuka T (2013) May-September precipitation in the Bhutan Himalaya since 1743 as reconstructed from tree ring cellulose δ 18 O. J Geophys Res-Atmos 118(15):8399–8410
Shi C, Daux V, Zhang Q, Risi C, Hou S, Stievenard M, Pierre M, Li Z, Masson-Delmotte V (2012) Reconstruction of Southeast Tibetan Plateau summer climate using tree ring δ18O: moisture variability over the past two centuries. Clim Past 8(1):205–213
Tian L, Masson-Delmotte V, Stievenard M, Yao T, Jouzel J (2001a) Tibetan Plateau summer monsoon northward extent revealed by measurements of water stable isotopes. J Geophys Res-Atmos 106(D22):28081–28088
Tian L, Yao T, Numaguti A, Sun W (2001b) Stable isotope variations in monsoon precipitation on the Tibetan Plateau. J Meteorol Soc Jpn. Ser II 79(5):959–966
Webster PJ, Palmer TN (1997) The past and the future of El Niño. Nature 390(6660):562–564
Wernicke J, Grießinger J, Hochreuther P, Bräuning A (2015) Variability of summer humidity during the past 800 years on the eastern Tibetan Plateau inferred from δ < sup > 18</sup > O of tree-ring cellulose. Clim Past 11(2):327–337
Wieloch T, Helle G, Heinrich I, Voigt M, Schyma P (2011) A novel device for batch-wise isolation of α-cellulose from small-amount wholewood samples. Dendrochronologia 29(2):115–117
Wu R, Chen J, Chen W (2012) Different Types of ENSO influences on the Indian summer monsoon variability. J Clim 25(3):903–920
Yang J, Liu Q, Liu Z (2010) Linking Observations of the Asian Monsoon to the Indian Ocean SST: Possible Roles of Indian Ocean Basin Mode and Dipole Mode. J Clim 23(21):5889–5902
Yao T, Thompson L, Yang W, Yu W, Gao Y, Guo X, Yang X, Duan K, Zhao H, Xu B, Pu J, Lu A, Xiang Y, Kattel DB, Joswiak D (2012) Different glacier status with atmospheric circulations in Tibetan Plateau and surroundings. Nat Clim Chang 2(9):663–667
Zhang Q, Evans MN, Lyu L (2015) Moisture dipole over the Tibetan Plateau during the past five and a half centuries. Nat Commun 6:8062